Hybrid Zinc Oxide Conjugated Polymer Bulk Heterojunction Solar Cells

Waldo J. E. Beek, Martijn M. Wienk, Martijn Kemerink, Xiaoniu Yang, and René A. J. Janssen*

Molecular Materials and Nanosystems, Departments of Chemical Engineering & Chemistry and Applied Physics, Eindhoven University of Technology, P.O. Box 513, 5600 MB Eindhoven, The Netherlands, and Dutch Polymer Institute, P.O. Box 902, 5600 AX Eindhoven, The Netherlands

Received: February 11, 2005

Bulk heterojunction photovoltaic devices based on blends of a conjugated polymer poly[2-methoxy-5-(3′,7′-dimethyloctyloxy)-1,4-phenylenevinylene] (MDMO−PPV) as electron donor and crystalline ZnO nanoparticles (*nc*-ZnO) as electron acceptor have been studied. Composite *nc*-ZnO:MDMO−PPV films were cast from a common solvent mixture. Time-resolved pump−probe spectroscopy revealed that a photoinduced electron transfer from MDMO−PPV to *nc*-ZnO occurs in these blends on a sub-picosecond time scale and produces a long-lived (milliseconds) charge-separated state. The photovoltaic effect in devices, made by sandwiching the active *nc*-ZnO:MDMO−PPV layer between charge-selective electrodes, has been studied as a function of the ZnO concentration and the thickness of the layer. We also investigated changing the degree and type of mixing of the two components through the use of a surfactant for ZnO and by altering the size and shape of the *nc*-ZnO particles. Optimized devices have an estimated AM1.5 performance of 1.6% with incident photon to current conversion efficiencies up to 50%. Photoluminescence spectroscopy, atomic force microscopy, and transmission electron microscopy have been used to gain insight in the morphology of these blends.

1. Introduction

The high costs of materials and production associated with multicrystalline silicon solar cell modules spurs the development of thin-film photovoltaic devices based on organic and polymer materials that can be manufactured by roll-to-roll technologies. In contrast to silicon and most conventional inorganic semiconductors, photoexcitation of organic semiconductors does not directly result in free charge carriers. Instead, a strongly bound electron−hole pair, or exciton, is generated.[1] This exciton can be separated to form free charge carriers at the interface between an electron-donor (*p*-type) and electron-acceptor (*n*-type) material. The exciton lifetime and its diffusion length in organic and polymer semiconductors are limited by radiative and nonradiative decay, and therefore only excitons generated in close vicinity of the *p*−*n* interface can give rise to charges. To boost charge generation, the interface area can be enlarged by intimately mixing the *p*- and *n*-type materials into a single layer or bulk heterojunction. The challenge in making bulk heterojunction solar cells is to find a balance between a high interface area for effective photogeneration of charges and an appropriate phase separation into continuous *p*- and *n*-type domains for effective transport of charges (holes and electrons) toward the electrodes. So far, organic bulk heterojunction solar cells have been made using polymer/fullerene,[2−7] polymer/polymer,[8−10] and molecular blends,[11−16] with maximum efficiencies of 3−4% under simulated solar light (AM1.5).

Conjugated polymers can also be combined with *n*-type inorganic semiconductors. Such hybrid polymer−inorganic nanocomposites may combine the advantages of both materials: solution processing of polymer semiconductors and the high electron mobility of inorganic semiconductors. Several hybrid

bulk heterojunction polymer solar cells have been reported including CdSe nanodots,[17,18] nanorods,[19] and tetrapods[20,21] and TiO₂ nanoparticles.[22] We recently described the successful combination of ZnO nanoparticles (*nc*-ZnO) and poly[2-methoxy-5-(3′,7′-dimethyloctyloxy)-1,4-phenylenevinylene] (MDMO−PPV), leading to solar cells with an estimated AM1.5 performance of 1.6%.[23] This efficiency is comparable to the highest efficiencies reported for hybrid-conjugated polymer devices. In fact, the *nc*-ZnO:MDMO−PPV devices surpass the other hybrid devices in terms of open circuit voltage (V_{OC}) and fill factor (FF),[24] and therefore the challenge is to improve the short-circuit current (J_{SC}) compared to the best devices made using MDMO−PPV and acceptors such as fullerenes[3,4] or CdSe.[19−21]

For all bulk heterojunction solar cells, the morphology of the active layer is crucial in the performance of these devices.[25−29] This paper aims at providing a deeper insight in the parameters that determine the performance of hybrid bulk heterojunction solar cells based on *nc*-ZnO and conjugated polymers such as MDMO−PPV. First, transient photoinduced absorption is applied to investigate the kinetics of charge separation and recombination across the *nc*-ZnO:MDMO−PPV interface. Then, photoluminescence spectroscopy, transmission electron microscopy (TEM), and tapping-mode atomic force microscopy (TM-AFM) are employed to study the morphology of the composite layers as a function of the amount of ZnO. We also change the mixing of the two components by using a surfactant for ZnO and by altering the size and shape of the *nc*-ZnO particles. Finally we address the stability of these devices in the presence of ultraviolet (UV) light.

2. Synthesis and Characterization of ZnO Nanoparticles

ZnO nanoparticles were synthesized by hydrolysis and condensation of zinc acetate dihydrate by potassium hydroxide

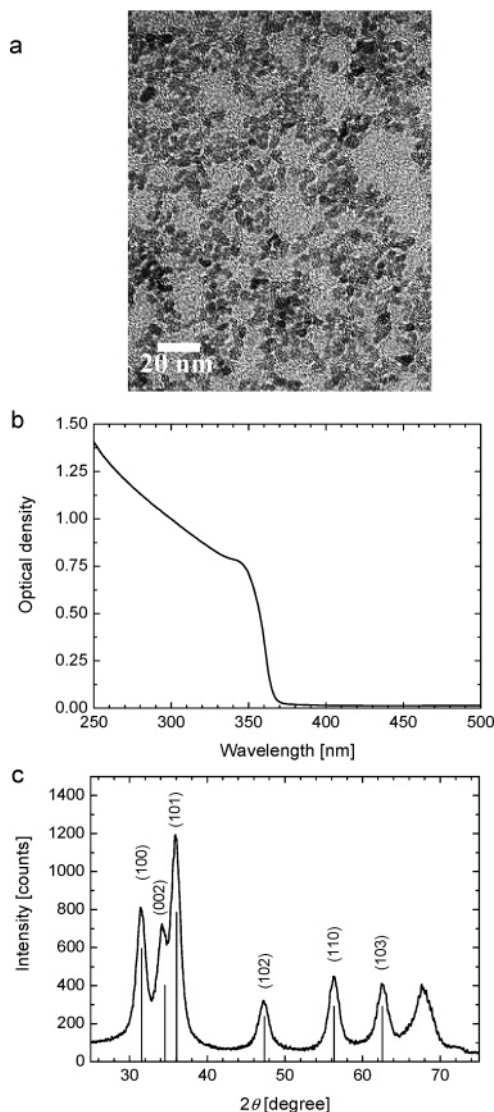* To whom correspondence should be addressed. E-mail: r.a.j.janssen@tue.nl.

Figure 1. ZnO nanoparticles prepared with a Zn^{2+}:OH^- ratio of 1.7. (a) TEM image. (b) UV–vis absorption spectrum in a chloroform:methanol (v:v = 90:10) mixture. (c) Powder XRD pattern.

in methanol using a Zn^{2+}:OH^- ratio of 1:1.7 according to Weller et al.[30] This procedure resembles methods previously described by Henglein et al.[31] and Meulenkamp.[32] The resulting ZnO nanoparticles are insoluble in pure methanol, but by addition of suitable amounts of less polar solvents such as dichloromethane, chloroform, or chlorobenzene, stable solutions are obtained. No additional surfactants or ligands are needed to disperse the ZnO nanoparticles in these solvent mixtures to reach solubility up to 75 mg mL^{-1}. TEM indicates that particles of 5 nm in diameter were obtained, which appear rather monodisperse (Figure 1a).

Because the extension of the electronic wave functions of semiconductor quantum dots is confined to the particle, their energy levels are size-dependent and UV–vis spectroscopy can be used to determine the diameter of semiconductor nanoparticles such as ZnO. Figure 1b shows the UV absorption spectrum of ZnO nanoparticles in a chloroform:methanol mixture. According to Meulenkamp,[32] the observed $\lambda_{1/2}$[33] of 360 nm corresponds to a particle diameter of 4.9 nm.[34] $\lambda_{1/2}$ levels off at approximately 365 nm after the nanoparticles reach a diameter of 6 nm.[32] This indicates that quantum confinement and its effect on the UV absorption onset is only present in smaller particles. Therefore the UV onset is not a measure for the size of bigger
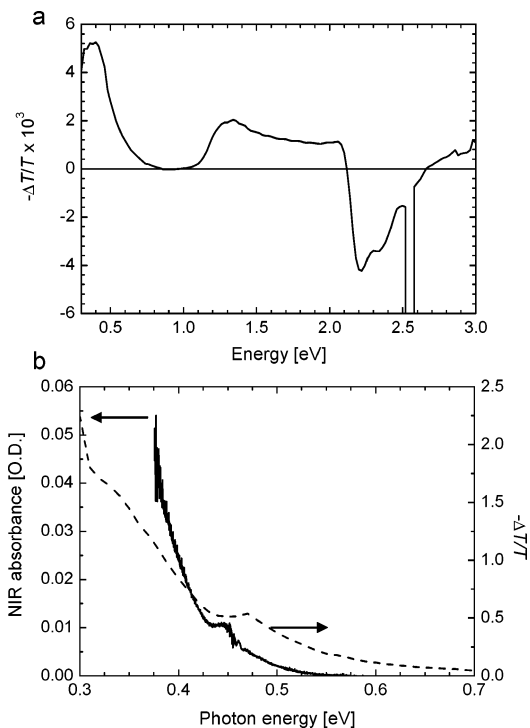

Figure 2. Near-steady-state PIA spectrum of: (a) *nc*-ZnO:MDMO–PPV blend (35 vol. % ZnO) on quartz, measured at 80 K with modulated (275 Hz) excitation at 2.54 eV (488 nm). The pump power was 25 mW with a beam diameter of 2 mm. (b) NIR absorption (left axis) and photoinduced absorption (right axis) spectra of a *nc*-ZnO film deposited on quartz. The NIR signal was recorded after exposure to a xenon lamp. The strong PIA signal was obtained by excitation the ZnO film with 350 and 363 nm, at 298 K exposed to air.

particles. The reflections in the X-ray diffraction (XRD, Figure 1c) confirm the formation of a wurtzite-type ZnO crystalline phase.[35]

3. Photoinduced Charge Transfer in *nc*-ZnO:MDMO–PPV

To investigate photoinduced charge separation in mixed *nc*-ZnO:MDMO–PPV layers, we have performed photoinduced absorption experiments from the sub-picosecond to the millisecond time domain. Thin film samples for these studies were made by spin casting a *nc*-ZnO:MDMO–PPV (35 vol. % *nc*-ZnO) mixture from chlorobenzene:methanol (v:v = 95:5) on quartz.

The near-steady-state photoinduced absorption (PIA) spectrum of a *nc*-ZnO:MDMO–PPV thin film, recorded with modulated (275 Hz) photoexcitation at 488 nm, exhibits a bleaching band of neutral MDMO–PPV at 2.2 eV and the characteristic absorption bands of the polymer radical cation around 0.4 and 1.3 eV (Figure 2a).[36] The intensity ratio of these bands is different from usual, and we attribute the higher intensity of the 0.4-eV band to an additional signal from electrons injected in ZnO.[37] The simultaneous observation of radical cations in MDMO–PPV and conduction band electrons in ZnO provides direct spectral evidence of a photoinduced electron-transfer reaction between these components. The PIA spectrum of *nc*-ZnO:MDMO–PPV shows strong resemblance to spectra of InP:MDMO–PPV and CdSe:MDMO–PPV blends observed by Pientka et al.[38] Also in these spectra, the low-energy absorption band has been attributed to injected electrons in the nanocrystals.
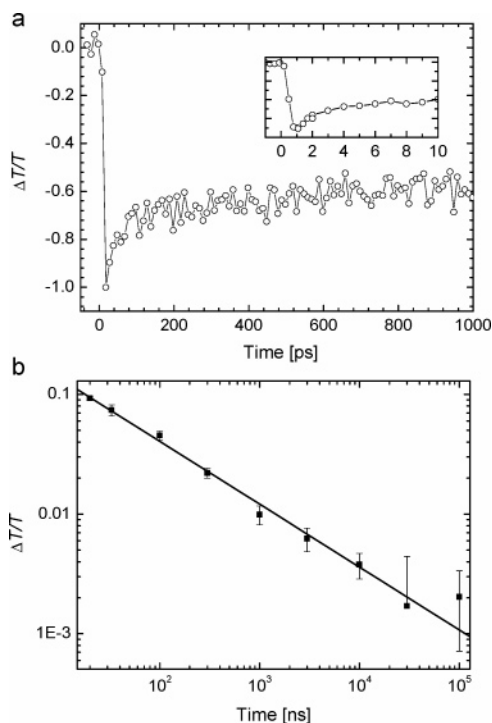
Bulk Heterojunction Solar Cells

J. Phys. Chem. B, Vol. 109, No. 19, 2005 **9507**

Figure 3. (a) Time-resolved pump−probe PIA spectroscopy measured at room temperature, monitoring the intensity of the MDMO−PPV radical cation band at 0.56 eV (2200 nm) after excitation at 2.43 eV (510 nm) with 200-fs pulses. The inset shows the transient absorption at short time delays. (b) Decay of the photobleaching band in an *nc*-ZnO:MDMO−PPV blend (26 vol. % ZnO) as a function of time. Excitation 2.76 eV (450 nm), pump fluence 1 mJ cm^{-2}.

This assignment is further corroborated by PIA experiments and near-infrared (NIR) absorption spectroscopy following UV illumination of a film containing only ZnO nanoparticles. After exposure of a pure ZnO nanoparticle film to light from a xenon lamp in an inert atmosphere, a weak NIR absorption is observed (Figure 2b).[39] Katoh et al. observed the same NIR absorption of ZnO nanocrystalline films after electron injection by sensitizers or UV exposure.[40] In the absence of oxygen, the NIR signal associated with conduction band electrons is stable for minutes. The PIA spectrum recorded with modulated UV excitation of a ZnO nanoparticle film also shows a strong signal in the NIR region. Interestingly, the strong PIA signal is only observed upon exposure of the ZnO particles to oxygen (from ambient air). The role of oxygen in the near-steady PIA experiment is to allow for a modulation of the concentration of conduction band electrons between on and off illumination time intervals by quenching these electrons. In the absence of oxygen, the long-lived conduction band electrons would remain undetected in the lock-in detection scheme used in this PIA technique. The results confirm that, with direct UV excitation, the conduction band electron in ZnO has a long lifetime, most likely as a result of trapping of the corresponding hole.[41,42] The result is an *n*-type doped ZnO nanoparticle.

The kinetics of charge generation has been studied with sub-picosecond pump−probe spectroscopy (Figure 3a) by monitoring the intensity of the low-energy radical cation absorption band at 2200 nm (0.56 eV). Upon excitation at 510 nm (2.43 eV) of MDMO−PPV with 200-fs pulses, the PIA signal rises within one picosecond, demonstrating an ultrafast forward electron transfer toward *nc*-ZnO. Similarly fast-electron injection (<300 fs) has been observed for Ru(dcbpy)$_2$(NSC)$_2$ dyes on nanoparticulate ZnO electrodes by Hagfeldt et al.[43]

Nanosecond photoinduced spectroscopy measurements on *nc*-ZnO:MDMO−PPV blends were performed to monitor the recombination of the photogenerated holes and electrons. Films were photoexcited with 4-ns pulses at 450 nm (2.76 eV). Figure 3b shows that the intensity of the photoinduced bleaching band at 2.2 eV decays with time following a power law ($\Delta T/T \propto t^{-0.53}$) from nanoseconds to milliseconds after excitation. This demonstrates that charge separation is long-lived and that the recombination kinetics are analogous to those in fullerene:polymer (PCBM:MDMO−PPV) blends, measured under identical conditions.[44] For the latter blends, it is assumed that recombination is limited by detrapping of the cationic charge carriers in MDMO−PPV.[44]

In summary, in *nc*-ZnO:MDMO−PPV blends, a fast forward and slow backward electron-transfer reaction occur upon excitation with visible light. These photophysical properties are beneficial for operation in photovoltaic devices.

4. Photovoltaic Performance and Morphology of *nc*-ZnO:MDMO−PPV Blends

In this section, we discuss the effect of the amount of *nc*-ZnO particles in the blend on the performance of the solar cells. UV−vis absorption spectroscopy has been used to confirm that the amount of ZnO used in solution correlates with the amount of ZnO in the blend. The efficiency of charge separation as a function of ZnO concentration in the blend has been monitored by photoluminescence quenching and by the collection of charges in photovoltaic devices. The morphology of the active layers has been studied to correlate the ZnO concentration with the performance of the devices.

4.1. UV−vis Absorption Spectroscopy. UV−vis absorption spectra were recorded to investigate the relation between the amount of ZnO added to the solution used for spin coating and the amount of ZnO in the resulting film. Addition of ZnO nanoparticles to the solution results in an increase of the ZnO absorption (below 400 nm) in the spectrum relative to the MDMO−PPV signal (λ_{max} = 505 nm) (Figure 4a). The absorption spectrum of MDMO−PPV does not change, and the optical density at the maximum stays roughly the same because the MDMO−PPV concentration was constant and only the ZnO concentration varied.

In a first approximation, the relation between the amount of ZnO in the blend and the ratio of the optical density of ZnO and the optical density of the MDMO−PPV is given by

$$\frac{OD_{ZnO}}{OD_{PPV}} = \frac{\alpha_{ZnO} \times L^{eff}_{ZnO}}{\alpha_{PPV} \times L^{eff}_{PPV}} \sim \frac{\text{vol. \% ZnO}}{100 - (\text{vol. \% ZnO})} \quad (1)$$

where L^{eff} is the effective path length, α the absorption coefficient, and vol. % ZnO the expected volume percentage of ZnO in the film based on the composition of the solution used for spin casting.[45] The data in Figure 4b show a good correlation between the amount of ZnO in the solution used for spin casting and the amount of ZnO in the film. By use of the absorption coefficient of MDMO−PPV (1.3×10^7 m^{-1})[46] and the slope of the plot in Figure 4b ($\alpha_{ZnO}/\alpha_{PPV}$ = 0.58), the absorption coefficient of the ZnO nanoparticles can be estimated to be $\alpha_{ZnO} = 7 \times 10^6$ m^{-1}. This absorption coefficient is higher than the value reported for ZnO crystals ($\alpha_{ZnO} \approx 10^6$ m^{-1})[47] in accordance with the fact that for quantum-confined nanoparticles the absorption coefficient shows a strong increase compared to its bulk value.[48]

4.2. Photoluminescence Spectroscopy. Before addressing the effect of the ZnO concentration on the performance of the
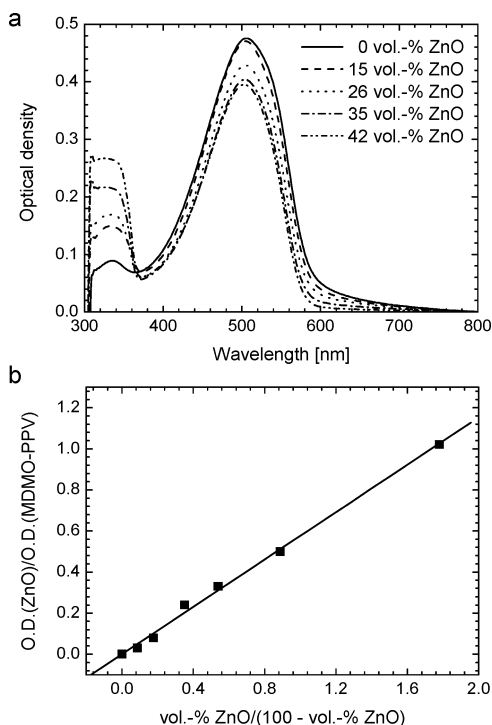
Figure 4. (a) UV−vis spectra of *nc*-ZnO:MDMO−PPV films bends spin cast at 1500 rpm (3 mg mL^{-1} MDMO−PPV) on PEDOT:PSS-covered ITO substrates. (b) Ratios of the optical density of ZnO (335 nm) and MDMO−PPV (505 nm) as function of the ratio of the vol. % ZnO.

Figure 5. (a) Photoluminescence spectra of *nc*-ZnO:MDMO−PPV blends, excitation performed at 505 nm. The intensities are corrected for the optical density of the films. (b) Time-resolved photoluminescence of the emission at 580 nm recorded with excitation at 400 nm. The data have been normalized at 10.000 counts.

photovoltaic devices, it is useful to see how this affects charge formation. Because of the fast, sub-picosecond forward electron-transfer reaction, mixing of ZnO and MDMO−PPV will result in a quenching of the photoluminescence of the polymer. Indeed, the spectra (Figure 5a) show that the photoluminescence of MDMO−PPV is increasingly quenched upon addition of ZnO. At 35 vol. % ZnO, 85% of the original MDMO−PPV photoluminescence intensity is lost. Because energy (exciton) transfer from the polymer to ZnO is highly endergonic, we attribute the fluorescence quenching to electron transfer, although a contribution from increased nonradiative decay (e.g., intersystem crossing) cannot be ruled out. From these results, we infer that a maximum of 85% of the absorbed photons leads to charge separation. Addition of more ZnO does not lead to a further quenching. The residual photoluminescence can be explained by assuming that phase separation between MDMO−PPV and ZnO occurs on a length scale larger than the exciton diffusion length (approximately 10 nm for MDMO−PPV). The time-resolved photoluminescence traces (Figure 5b) show a decrease of the fluorescence lifetime of the residual MDMO−PPV emission with increasing amount of ZnO in the film. The reduced lifetime can be explained by assuming that at higher concentrations (up to 42 vol. %) more photoexcitations in MDMO−PPV are generated close to the interface with ZnO and therefore require less diffusion before charge separation can occur.

4.3. Photovoltaic Devices. To study the effect of the ZnO concentration in the film on photovoltaic performance, hybrid *nc*-ZnO:MDMO−PPV devices with different amounts of *nc*-ZnO were prepared and investigated by recording the *J*−*V* characteristics under illumination. The devices were made by spin casting *nc*-ZnO:MDMO−PPV from solution into thin films on a transparent hole collecting electrode consisting of a glass substrate, coated with indium tin oxide (ITO) and poly(3,4-ethylenedioxythiophene):poly(styrenesulfonate) (PEDOT:PSS).
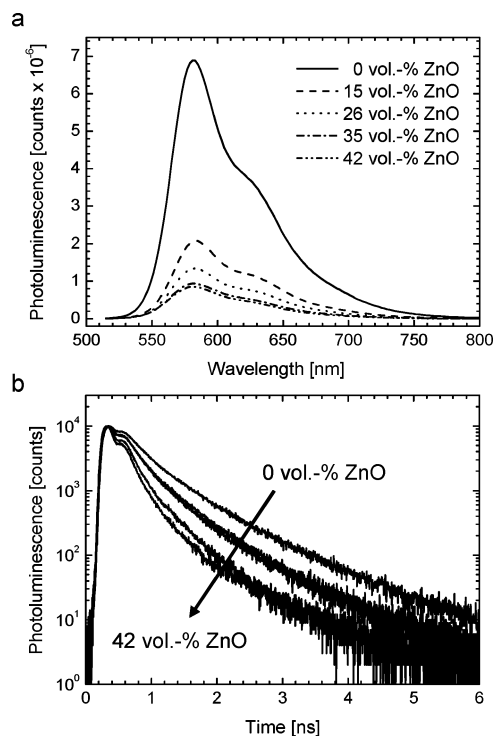
The devices (0.1 cm^2 area) were completed by thermal evaporation of a 100 nm thick aluminum layer and characterized in inert atmosphere nitrogen (<1 ppm H$_2$O, < 1 ppm O$_2$). The experiments were performed in a short period of time to rule out variations in performance due to changes in the surrounding atmosphere.[49] The effects of the ZnO concentration and layer thickness on the maximum power point (MPP) under white light illumination are shown in Figure 6. The maximum performance is observed for devices containing 26−35 vol. % ZnO and a layer thickness between 100 and 150 nm. Devices containing higher amounts of ZnO (47 vol. %) appear to have their optimal performance at higher layer thickness.

For a meaningful evaluation, *J*−*V* characteristics of devices with the same layer thickness should be compared. Parts c and d of Figure 6 show the *J*−*V* characteristics for cells with different vol. % of ZnO and a constant layer thickness of approximately 100 nm. Several characteristics can be noted. Figure 6c shows that open circuit voltage (*V*$_{OC}$) decreases with increasing amount of ZnO. This might be related to the formation of shunts; relatively well conducting pathways of ZnO particles from electrode to electrode, whose likelihood increases when the amount of ZnO increases. In accordance with this explanation, an increase in layer thickness results in an increase of *V*$_{OC}$ when the amount of ZnO is constant (data are not shown). The short circuit current (*J*$_{SC}$) initially increases when the amount of ZnO in the blend is increased. This trend can be explained by the increased formation of charges inferred from the photoluminescence quenching (Figure 5a). An additional effect might be the formation of more percolation pathways of ZnO nanoparticles that improve the transport of electrons and increase the photocurrent. Keeping the layer thickness constant but increasing the amount of ZnO leads to a decrease of the absorption of light by MDMO−PPV, which rationalizes the
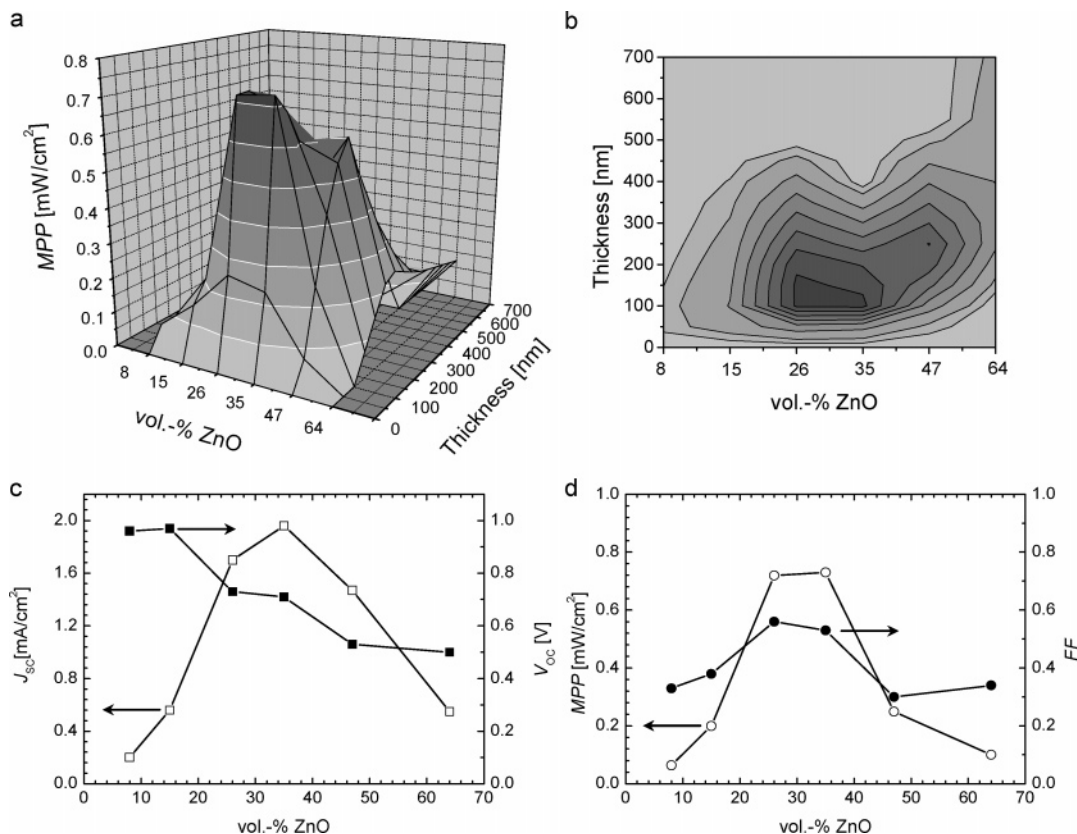
Bulk Heterojunction Solar Cells

J. Phys. Chem. B, Vol. 109, No. 19, 2005 **9509**

Figure 6. The MPP value of *nc*-ZnO:MDMO−PPV solar cells, as a function of vol. % ZnO and the thickness of the active layer. (a) Three-dimensional representation and (b) a top view of the same image. The bottom graphs show how J_{SC} (c), V_{OC} (c), FF (d), and MPP (d) depend on the vol. % ZnO for *nc*-ZnO:MDMO−PPV solar cells with a layer thickness of 100 nm.

decrease of the short circuit current at higher vol.-% of ZnO nanoparticles.

The FF ranges from 0.3 to 0.6 depending on the amount of ZnO in the blend. The observed maximum can be explained by reasoning that the FF is a measure for the balance between hole and electron transport. At low ZnO concentrations, electron transport is poor; at high ZnO concentration, the polymer phase is highly diluted and hole transport is poor. The low FF at a high vol. % of ZnO can also be related to a low shunt resistance, which was also used to explain the trend in V_{OC}. The overall trend, when all parameters are combined into the MPP is that the optimal amount of ZnO is approximately 30 vol. % (or 70 wt. % ZnO). This is less than the optimal amounts required for fullerenes (PCBM) in PCBM:MDMO−PPV blends (80 wt. %)[2] and 90 wt. % for CdSe nanoparticles and rods[17−19] blended with *rr*-P3HT and MDMO−PPV.

Current density−voltage (*J*−*V*) characteristics of the best devices are shown in Figure 7a. These exhibit a good diode behavior (rectification ratio is 3×10^4 at ± 2 V). Light intensity dependent *J*−*V* measurements, performed with white-light illumination and a set of neutral density filters, reveal a sublinear relation of J_{SC} with light intensity (*I*) ($J_{SC} \propto I^n$, with $n = 0.93$) (Figure 7b), an increase of V_{OC} with *I* (ultimately reaching more than 800 mV), and an increase of FF up to values close to 0.6. The incident photon to current conversion efficiency (IPCE, Figure 7c) measured with white-light bias illumination resembles the absorption spectrum of the *nc*-ZnO:MDMO−PPV layer on glass and reaches 40% at the absorption maximum MDMO−PPV. Integration of the spectral response with the solar spectrum (AM1.5G, normalized 100 mW cm^{-2}) provides an estimate of the short-circuit current density ($J_{SC} = 3.3$ mA cm^{-2}) under AM1.5 (1 sun) conditions. The *J*−*V* curve, measured at $I = 0.71$ sun equivalent[50] white-light illumination using a tungsten−

halogen lamp, is shown in Figure 7a. Under these conditions $J_{SC} = 2.40$ mA cm^{-2} is obtained, together with $V_{OC} = 814$ mV and FF = 0.59, leading to an estimated overall power conversion efficiency (η) of 1.6% at this light intensity.

4.4. Morphology of *nc*-ZnO:MDMO−PPV Composite Films. In virtually all bulk heterojunction devices, the morphology of the phase separation is one of the key parameters in achieving an optimum performance. The optimum morphology is a critical balance between a well-dispersed system for efficient charge separation and a phase separation on a large scale to improve charge transport. Here we study the morphology of the *nc*-ZnO:MDMO−PPV blends with TEM and TM-AFM.

4.4.1. TEM. Thin layers of the *nc*-ZnO:MDMO−PPV blends have been investigated with TEM. The specimens were prepared by spin coating the photoactive blend on top of PEDOT:PSS as in normal device preparation and subsequently separating the active layer from the PEDOT:PSS layer by flotation on water and transfer to a TEM grid.

The higher electron density of the ZnO nanoparticles compared to MDMO−PPV gives rise to contrast in the TEM images, and hence the dark regions in Figure 8a indicate the presence of ZnO nanoparticles. At 100 nm thickness, the 26 vol. % ZnO blend shows no coarse phase segregation and appears rather homogeneous. However, in a 100 nm thick film, the transmission may be obscured by shadowing effects of ZnO nanoparticles. Therefore a thinner film (50 nm) was investigated (Figure 8b). The corresponding TEM image (Figure 8b) reveals that phase separation on a nanometer scale exists, because regions can be observed where almost no ZnO nanoparticles can be detected. The presence of pure MDMO−PPV regions, some bigger than 10 nm (the approximate exciton diffusion length in PPV), is consistent with the residual photoluminescence observed in these blends ZnO (Figure 5a).
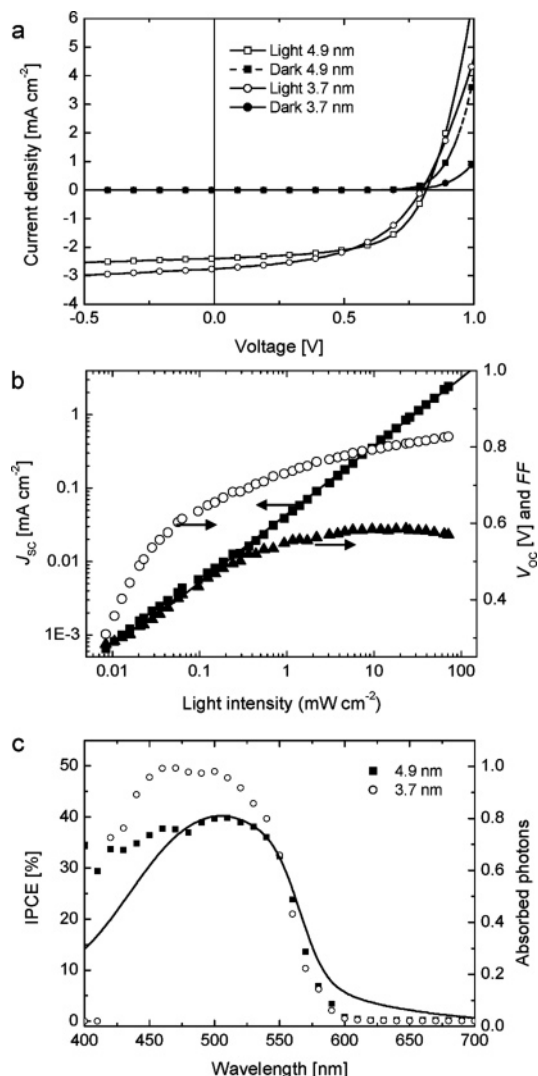
Figure 7. Photovoltaic device characterization of a *nc*-ZnO:MDMO−PPV (26 vol. % *nc*-ZnO) solar cells with 4.9- and 3.7-nm ZnO nanoparticles (sizes based on UV absorption onset). (a) *J*−*V* characteristics in the dark (solid symbols) and under illumination with white light from a tungsten halogen lamp estimated at 0.71 sun equivalent intensity (open symbols) for 4.9 nm (squares) and 3.7 nm (circles) particles. (b) Evolution J_{SC} (squares) with least-squares fit of power-law behavior (solid line), V_{OC} (open circles), and *FF* (triangles) as a function of light intensity. (c) IPCE as function of the wavelength of monochromatic irradiation for 4.9- (solid squares) and 3.7-nm (open circles) particles, co-plotted with the fraction of photons absorbed by the blend.

4.4.2. TM-AFM. The TEM images of *nc*-ZnO:MDMO−PPV blends indicate that the blends are phase segregated on a nanometer scale. Studying the surface morphology of thin films can reveal further information on the distribution of phases. TM-AFM can give information about the height differences and, via the phase image, also about the composition of the materials at the surface. However, interpretation of height and phase images is not straightforward, because they are influenced by parameters such as tapping force, tip shape, and quality, humidity, and the nature of the sample itself (e.g., hydrophobic, hydrophilic, tacky).[51−53] Because hard nanoparticles can easily be distinguished from the soft polymer, hybrid mixtures seem ideally suited to study with TM-AFM. However, there are only a few examples of TM-AFM on blends from nanoparticles and (conjugated) polymers.[27] In one study on SiO$_2$ nanoparticles in a PVP (poly[*n*-vinyl-2-pyrrolidone]) film, it has been reported
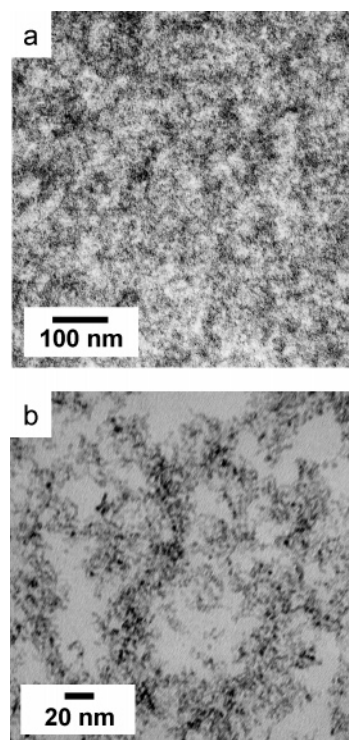

Figure 8. TEM photographs of (a) a thin (100-nm) film of an *nc*-ZnO:MDMO−PPV blend with 26 vol. % ZnO and (b) a 50-nm thin film of the same blend.

that it is possible to detect SiO$_2$ particles 5−7 nm beneath the surface of the PVP film.[54]

The TM-AFM phase image recorded for a blend with 8 vol. % ZnO (Figure 9) shows a strong, reversible dependence on tapping force. Because the phase shift of the cantilever oscillation is related to the power dissipated in a nonelastic tip−sample interaction,[55,56] a hard material generally shows a positive phase shift with respect to a soft material, and therefore the bright areas in Figure 9 are interpreted as the harder material and the dark areas as the softer material.

The TM-AFM phase images in Figure 9 show the effect of the tapping force on the phase image. Soft tapping (Figure 9a) shows a mostly soft material. Upon increase of the tapping force (parts b and c of Figure 9), more hard material becomes visible. The images can only be interpreted by assuming that there is a soft layer of MDMO−PPV on top of a harder material. Upon increase of the tapping force, this surface layer is penetrated and the harder underlying material is observed as a positive phase shift.

In the height images, the "disappearance" of the top layer by harder tapping can also be observed. In Figure 10a (soft tapping), the surface appears partially "wetted" with a thin film. Part of this wetting disappears with an increase in the tapping force (Figure 10b) and is no longer visible in the height image. The part of the "wetted" surface layer that remains visible in the height image appears dark in the phase image (see the inset in Figure 10b), i.e., this appears to be a soft material. From the height cross sections, the thickness of the top layer was estimated to be 1−2 nm, and we infer that it must be pure MDMO−PPV because the 5 nm sized ZnO nanoparticles cannot be imbedded in this 1−2-nm thin film. We note that these effects on the height and phase images were completely reversible; decreasing the tapping force restored the top layer.

The surface layer appears to be more pronounced in the blends with large amounts of MDMO−PPV. This might add up to the
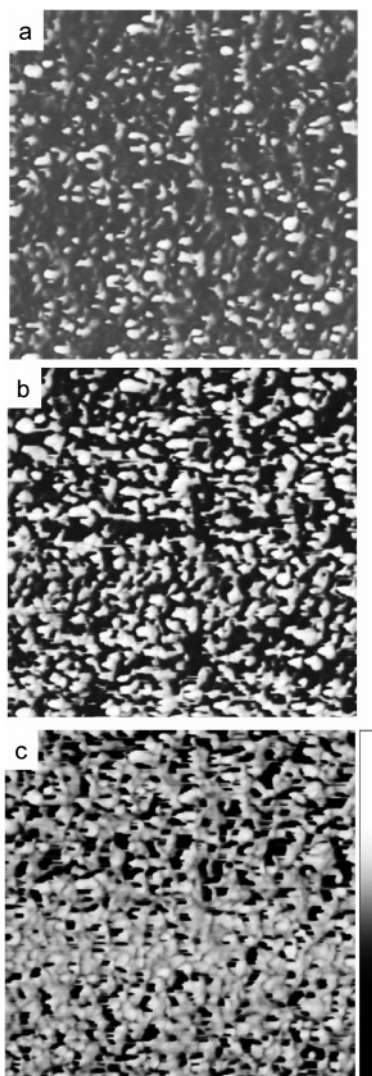
Bulk Heterojunction Solar Cells

J. Phys. Chem. B, Vol. 109, No. 19, 2005 **9511**

Figure 9. TM-AFM phase images (500 nm × 500 nm) of *nc*-ZnO: MDMO−PPV blends with 8 vol. % ZnO. Vertical scale bar is 0−200°. The tapping force has been varied from (a) $I/I_0 = 0.6$ (lowest force) to (b) $I/I_0 = 0.5$ and (c) $I/I_0 = 0.45$ (highest force), were I_0 is the free amplitude and I the cantilever amplitude during image recording.

Figure 10. TM-AFM height images (500 nm × 500 nm) of *nc*-ZnO: MDMO−PPV blends with 4 vol. % ZnO, the vertical scale bar indicates 40 nm. (a) soft tapping, $I/I_0 = 0.6$ and (b) harder tapping, where $I/I_0 = 0.4$. The inset shows a phase image of the section bound by the dotted line.

observation that these blends show a smaller photovoltaic effect. The presence of a polymer layer between the active blend and the top electrode will act as a blocking layer for electron injection into this electrode and therefore leads to lower currents under illumination. We also observed that the polymer layer increases in thickness when the blend is stored (in a glovebox), probably because of diffusion of the polymer toward the top surface.

Although intriguing, this surface layer makes interpretation of the phase images challenging. Soft tapping is required to get a proper view on the actual surface morphology of these blends, because the topography of the samples is in some cases disturbed when larger tapping forces have been applied. The effect of the ZnO content on the surface morphology of the blends is shown in Figure 11. The height images in parts a−d of Figure 11 (under soft tapping conditions) are independent of the tapping force (I/I_0), apart from the effects related to the "wetted" surface layer. The corresponding phase images do not show any phase contrast other than due to the surface layer. In parts e and f of Figure 11, no surface layer has been observed, and the material appears to consist of a single homogeneous phase.
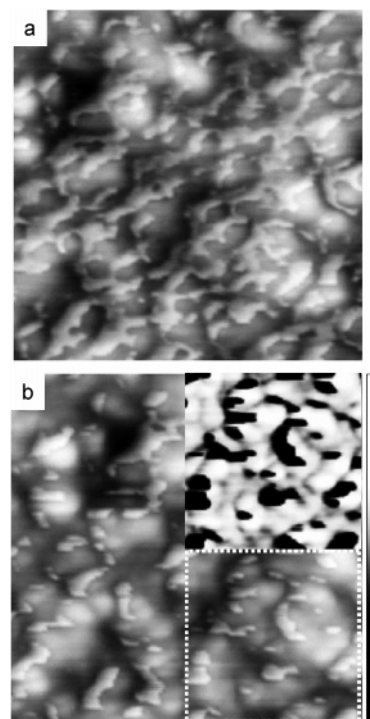
Blends with low amounts of ZnO (8 vol. %, Figure 11a) show a smooth surface (root-mean-square roughness is 2 nm, maximum height difference 12 nm), with a faint appearance of spherical aggregates. Parts b and c of Figure 11 show that with increasing ZnO content these faint structures are replaced by more spherelike structures. Increasing the ZnO content above 26−42 vol. % results in coagulation, growth of the spherical structures, and a significant increase in surface roughness. For blends with more than 15 vol. % ZnO, the AFM surface topography gives the impression that the film consists of an agglomerate of these spherical structures. It is possible that these have already been formed in solution prior to spin casting and that upon removal of the solvent the remaining polymer chains in solution adhere to the outside of the spherical structures. Interestingly, the rough phase, formed in blends with high amounts of ZnO, appears homogeneous because no phase contrast could be observed. This would imply that in the spherical features MDMO−PPV is (homogeneously) mixed with the ZnO nanoparticles or, alternatively, that at high vol. % ZnO pure ZnO particles are present at the surface.

We note that, although the TEM and TM-AFM studies give some important insights, they are not completely decisive. The TEM image of a thin film clearly shows the presence of MDMO−PPV domains without ZnO (Figure 8b) consistent with the fluorescence experiments, but this phase-separated system is not clearly identified with TM-AFM. In the same way, the spherical aggregates observed with TM-AFM are not observed in the TEM images. TM-AFM shows that small amounts of ZnO can be rather homogeneously blended with MDMO−PPV and that the size of the features and the roughness of the films increase when the amount of ZnO is increased (Figure 11). The trends observed for the photovoltaic effect as a function of the vol. % ZnO in the blend can partially be related to the morphology observed with TM-AFM. Upon addition of more
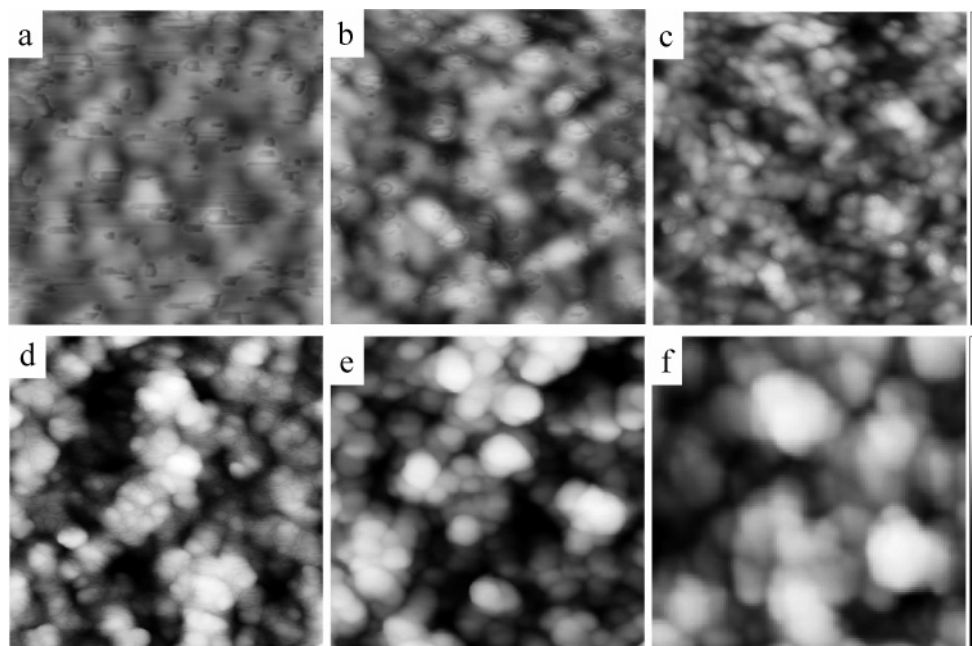
Figure 11. TM-AFM height images (500 nm × 500 nm): (a–c) 50 nm height bar and (d–f) 100 nm height bar. (a) 8 vol. % ZnO, 70 nm thick, 3 vol. % MeOH, roughness 2 nm (rms). (b) 15 vol. % ZnO, 90 nm thick, 2.2 vol. % MeOH, roughness 1.6 nm (rms). (c) 26 vol. % ZnO, 140 nm thick, 4 vol. % MeOH, roughness 4.0 nm (rms). (d) 42 vol. % ZnO, 220 nm thick, 5 vol. % MeOH, roughness 11 nm (rms). (e) 49 vol. % ZnO, 240 nm thick, 7 vol. % MeOH, roughness 19 nm (rms). (f) 64 vol. % ZnO, 350 nm thick, 10 vol. % MeOH, roughness 12 nm (rms).

TABLE 1: Summarized Results on Solar Cells Made Using *n*-Propylamine (PA), ZnO Nanoparticles, and ZnO Nanorods

no.	solvent[a]	spin speed (rpm)	vol. % ZnO		vol. % PA	J_{SC} (mA cm^{-2})	V_{OC} (V)	FF	MPP (mW cm^{-2})
1	CB	1500	26		0	2.46	0.78	0.58	1.1
2	CB	1500	26		0.5	2.1-2.2	0.6-0.7	0.50	0.7
3	CB	1500	8		2	1.1	0.78	0.48	0.4
4	CB	1500	26		2	1.5-1.6	0.6-0.7	0.59	0.6
5	CB	1500	35		2	1.9-2.1	0.64	0.55	0.7
6	CB	1000	26	rods	4	1.4	0.54	0.58	0.4
7	CB	1500	26	rods	4	1.1	0.52	0.62	0.4
8	CB	1000	35	rods	4	1.6	0.50	0.59	0.5
9	CB	1500	35	rods	4	1.2	0.47	0.61	0.3
10	CHCl$_3$	1500	26		2	1.6	0.65	0.52	0.5
11	CHCl$_3$	2000	26		2	1.3	0.64	0.51	0.4
12	CHCl$_3$	1500	26	rods	2	1.7	0.56	0.53	0.5
13	CHCl$_3$	2000	26	rods	2	1.6	0.56	0.53	0.5

[a] Solvents used: CB = chlorobenzene, CHCl$_3$ = chloroform. The vol. % *n*-propylamine is the amount added to the stock ZnO nanoparticle solution.

ZnO, spherical features are formed and these appear interconnected. Increasing the ZnO amount further eventually results in very rough films, i.e., the 64 vol. % ZnO blend (350 nm thick) has a surface height difference of approximately 100 nm. Solar cells made from these films show poor behavior because the absorbance of light (at constant thickness) is decreased and because thin films likely contain pinholes leading to shunts.

5. Effect of Surfactant, Shape, and Size of Nanoparticles in Hybrid Devices

In the previous sections, it was shown that both morphology and performance are strongly dependent on the amount and the dispersion of ZnO in the MDMO−PPV film. Here we address three methods to influence the dispersion of ZnO in the blend: (i) the use of surfactants to disperse the ZnO particles, (ii) the use of ZnO nanorods instead of nanoparticles to enhance transport, and (iii) the use of smaller ZnO particles.

5.1. *n*-Propylamine as Surfactant. In general, application of surfactants in photovoltaic devices based on nanoparticles is unfavorable because they hamper the electron-transfer process over the interface between the nanoparticle and the polymer

and the conductivity of the percolating nanoparticle network. Because *n*-propylamine is such a small molecule, effects such as these may be negligible. As shown in the previous sections, the homogeneity of nc-ZnO:MDMO−PPV blends is limited and very sensitive to the conditions during spin coating. We found that, upon addition of *n*-propylamine to the ZnO nanoparticle solution, films appear completely smooth by eye. This major improvement of film quality and reproducibility might provide improved photovoltaic devices. Table 1 summarizes experiments performed on several cells made using *n*-propylamine (entries 1−5) and shows that J_{SC} and V_{OC} decrease when the amount of *n*-propylamine in the ZnO sol is increased from 0.5 to 2 vol. %. J_{SC} can be slightly restored by increasing the amount of ZnO but results in a concomitant loss in V_{OC}. Even though addition of *n*-propylamine improves the film-forming properties of the blend, it does not lead to an improved performance of the solar cell.

5.2. ZnO Nanorods. Application of nanorods can lead to an improved transport of electrons through the nanoparticle network, because less electron hopping steps between individual nanoparticles are needed to bridge the distance to the collecting
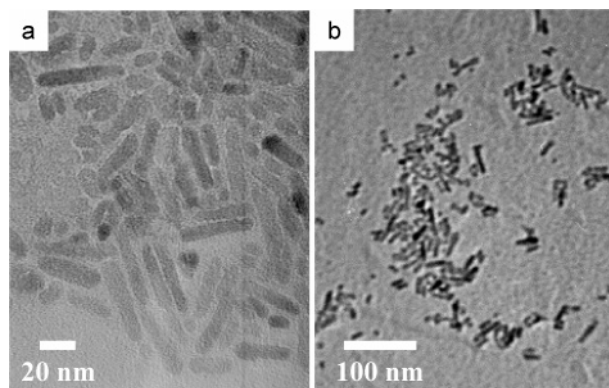
Bulk Heterojunction Solar Cells

J. Phys. Chem. B, Vol. 109, No. 19, 2005 **9513**

Figure 12. TEM images of rods prepared after heating a concentrated solution of ZnO nanoparticles for 20 (a) and 15 h (b).

electrode. This approach has been successful for polymer:CdSe cells, where the use of rods and tetrapods was shown to improve J_{SC}.[19,20] Hence, the application of ZnO nanorods seems a plausible approach to improve *nc*-ZnO:MDMO−PPV devices. Weller et al.[30] described that ZnO nanorods can be grown from the nanoparticles by heating a concentrated nanoparticle solution. The length of the rods can be tuned varying the heating time. Nanorods prepared at 60 °C for 20 h are up to 60 nm in length (Figure 12a) while heating for 15 h gives nanorods of approximately 25 nm (Figure 12b). The rods synthesized after 15 and 20 h both give a similar UV absorption with a $\lambda_{1/2}$ value of 365 nm corresponding to bulk ZnO. Compared to nanoparticles, the solubility of ZnO nanorods rods is rather low and they can only be dispersed in organic solvents with the aid of a small amount of *n*-propylamine. In chlorobenzene, 4 vol. % of *n*-propylamine is necessary to give barely stable solutions. ZnO nanorods can be dissolved in chloroform with smaller amounts of *n*-propylamine (2 vol. %), and these solutions show an improved long-term stability.

Solar cells made from ZnO nanorods (entries 6−9, Table 1) from chlorobenzene do give a photovoltaic effect, but J_{SC} and V_{OC} are reduced compared to the best nanoparticle based devices. Photovoltaic devices, prepared from rod and nanoparticle solutions in chloroform with the same amount of *n*-propylamine, have been compared to investigate the influence of the shape of the particle more directly. Table 1 (entries 10−13) reveals only minor differences in the performance of photovoltaic devices made using rods and nanoparticles. This demonstrates that photovoltaic devices with ZnO nanorods can be prepared but that, for a full utilization of the advantages of these rods, solubility in organic solvents without the application of surfactants seem to be required.

5.3. Smaller ZnO Nanoparticles. The size of the nanoparticles can be increased by raising the precursor concentration in the starting solution and by increasing the reaction time.[57] The size of the particles also strongly depends on the Zn^{2+}: OH^- ratio used in the synthesis. The ratio of 1:1.7 used in this work gives stable colloidal solutions with 5-nm particles. Increasing the Zn^{2+}:OH^- ratio from 1:1 to 1:1.75 results in larger particles, while a further increase of the ratio leads to smaller particles, and at a ratio of 1:2.5, the sol becomes unstable.[57]

Solar cells have also been made with nanoparticles made using a Zn^{2+}:OH^- ratio of 1:1.85 to decrease the size of the ZnO nanoparticles. The size of these nanoparticles determined from UV spectroscopy was 3.7 nm. TEM images of these particles were inconclusive, indicating that very small, but not nicely monodisperse, particles were formed. When introduced
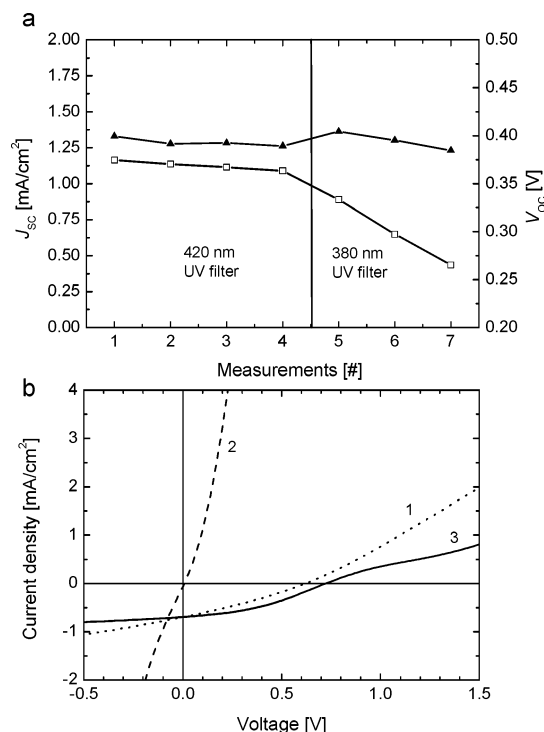

Figure 13. The effect of UV illumination on the performance of *nc*-ZnO:MDMO−PPV solar cells. (a) *nc*-ZnO:MDMO−PPV cell spin cast from chloroform as solvent, with 35 vol. % ZnO, indicating the effect of consecutive measurements on the short circuit current (▲, left axis) and open circuit voltage (□, right axis). (b) An *nc*-ZnO:MDMO−PPV solar cell with a 600 nm thick active layer containing 64 vol. % ZnO in MDMO−PPV. Curve 1 shows the initial solar cell performance. Curve 2 shows the same cell after short time UV illumination and curve 3 after exposure to air for 1 min.

in MDMO−PPV, these nanoparticles gave very nice photovoltaic devices. IPCE values up to 50% (at 500 nm) have been measured. By use of the IPCE, a 1 sun equivalent short circuit current density of 3.9 mA cm^{-2} was obtained (Figure 7c). Combined with the V_{OC} = 0.80 V and FF = 0.50 (measured at 0.71 sun equivalents, Figure 7a) this leads to a photovoltaic device with an efficiency of 1.56%, close to the maximum efficiency found for 4.9 nm sized particles.[23] The remarkable high current indicates that the size of the nanoparticles might be important for further optimization of the solar cell performance and that increasing the size of the nanoparticles or application of nanorods might not necessarily be the only way to improve charge transport.

6. Effect of UV Light on *nc*-ZnO:MDMO−PPV Solar Cells

When ZnO nanoparticles are directly excited across the band gap by UV excitation, they produce a mobile electron in the conduction band (see Figure 2b) and a deeply trapped hole. This effect is the origin for the photoluminescent behavior in the visible region of ZnO nanoparticles.[41,42] The sensitivity of ZnO toward UV light is a disadvantage of hybrid *nc*-ZnO:MDMO−PPV blends in solar cells because it deteriorates the performance. Figure 13a shows that, in absence of UV light, by placing a 420 nm cutoff filter between the cell and the light tungsten−halogen lamp, the $J-V$ characteristics are stable in time. However, V_{OC} decreases in consecutive measurements when a 380-nm cutoff filter is used to block UV light (Figure 13a). Longer illumination times, even with small amounts of UV light, lead to a complete loss of V_{OC}.

The effect of UV illumination has also been investigated for a device containing a thick layer of a blend with 64 vol. % ZnO in MDMO−PPV (Figure 12b). For this device, the $J-V$ curve before UV exposure (curve 1) is characterized by $J_{SC} = 0.7$ mA cm^{-2} and $V_{OC} = 0.62$ V. Illumination using a tungsten−halogen lamp without any UV filter results within seconds in a complete loss of V_{OC}, J_{SC}, and diode behavior (curve 2). Instead, the layer acts as a conductor. Surprisingly, exposure of this device to air for one minute restores J_{SC} and even slightly improves V_{OC}. This remarkable recovery can be related to the observations for ZnO nanoparticles in Figure 2b. Exposure to oxygen removes the electrons from the conduction band and restores the semiconducting properties of the ZnO phase.

7. Conclusions

Blends of crystalline ZnO nanoparticles and a conjugated polymer (MDMO−PPV) have been considered as the active layer for hybrid polymer solar cells. Transient photoinduced absorption (PIA) spectroscopy on mixed *nc*-ZnO:MDMO−PPV films reveal the formation of MDMO−PPV radical cations and conduction band electrons in *nc*-ZnO after excitation of the polymer with visible light. The photoinduced charge separation occurs within 1 ps and provides long-lived charge carriers that can be detected up to milliseconds after excitation. The photoluminescence quenching of MDMO−PPV maximizes at 85% for blends containing 35 vol. % ZnO or more. We conclude that, under these conditions, most, but not all, absorbed photons provide charges. From TEM and fluorescence lifetime studies, we infer that phase separation is responsible for the incomplete charge formation. As expected, the performance of the *nc*-ZnO:MDMO−PPV solar cells depends on the concentration of ZnO and the thickness of the active layer. The best performance is found for a blend with 30 vol. % ZnO and thickness of ∼100 nm, sandwiched between a transparent (PEDOT:PSS on ITO) and a metal (aluminum) electrode. These devices provide a photovoltaic effect with an estimated efficiency of about 1.6% under AM1.5 conditions. The morphology of the *nc*-ZnO:MDMO−PPV blends has been examined with TEM and TM-AFM. With TM-AFM, a thin layer covering the surface has been identified as MDMO−PPV.

Improving the solubility, stability, and miscibility of the nanoparticles by the addition of *n*-propylamine does not enhance the photovoltaic effect, which is rationalized by a loss in electron transport across the surfactant interface layer. Replacing nanoparticles with nanorods does not improve the performance, most likely because ZnO nanorods are more difficult to disperse in organics apolar solvents and require the addition of *n*-propylamine. Smaller ZnO particles (<4 nm based on UV−vis) give higher currents but a lower FF value in devices, making the over all performance similar to the larger particles.

One drawback of these devices is that small amounts of UV light (<420 nm) result in a rapid degradation of the photovoltaic effect. Formation of *n*-doped ZnO nanoparticles by direct band gap excitation and trapping of the hole is responsible for this effect. Fortunately, the electrons in the conduction band of the nanoparticles can be removed by exposure to oxygen, which restores the photovoltaic effect.

In summary, our studies have provided a deeper understanding of the photovoltaic properties of *nc*-ZnO:MDMO−PPV blends and demonstrate that reasonably efficient photovoltaic devices can be obtained with ZnO nanoparticles of different size and shape. TEM and TM-AFM have provided the first insights in the morphology of *nc*-ZnO:MDMO−PPV blends and show that a subtle interplay exists between the amount of ZnO

in the blend, the morphology, and the photovoltaic performance. A deeper understanding and, especially, control over the complex morphology of *nc*-ZnO:conjugated polymer blends will aid in improving the photovoltaic effect of this combination of materials.

8. Experimental Section

Materials. MDMO−PPV, synthesized via the Gilch route, was provided by Philips Research Eindhoven. MDMO−PPV has $M_w = \sim 1 \times 10^6$ g mol^{-1} and a polydispersity of about 7 as determined by size-exclusion chromatography calibrated against polystyrene. PEDOT:PSS was purchased from Bayer AG (Baytron P VPAI 4083) and aluminum wire (99.999%) from Engelhard-Clal.

ZnO Nanoparticles Synthesis. ZnO nanoparticles were prepared using an adapted procedure based on the work of Weller et al.[30] The general procedure used for the preparation of nanoparticles was as follows: zinc acetate dihydrate (Acros, >98%, 2.95 g, 13.4 mmol) was dissolved in methanol (125 mL) at 60 °C, a solution of KOH (Merck, 87%, 1.48 g, 23 mmol) in methanol (65 mL) was added in 10 min to the zinc acetate dihydrate solution under vigorous stirring. Zinc hydroxides precipitated but dissolved again. After 5 min, the solution became translucent and remained translucent. After 1.5 h, the nanoparticles started to precipitate and the solution became turbid. After 2 h and 15 min, the heater and stirrer were removed and the nanoparticles were allowed to precipitate for an additional 2 h. Precipitate and mother liquor were separated, and the precipitate was washed twice with methanol (50 mL). After the washing steps (5 min), the suspension was left unstirred for a minimum of 1 h to reach full precipitation. The washed precipitate was treated with chloroform or chlorobenzene (10 mL) to dissolve the nanoparticles. This solution was only slightly translucent, almost transparent, and was stable for more than two weeks. The amount of methanol in the resulting solution was determined with ^{1}H NMR. Replacing the last washing step with a centrifugation step (4300 rpm, 5 min) decreased the amount of methanol with a factor 2.

ZnO Nanorods Synthesis. The synthesis for the nanoparticles was followed up to the point of the precipitation step. After reaction for 2 h and 15 min, the reaction mixture was concentrated 10 times by solvent evaporation at 30 °C. The precipitate dissolved again, and the clear solution was heated at 60 °C for 15 or 20 h. During heat treatment, the nanorods started to precipitate. After heat treatment, methanol (50 mL) was added and the ZnO rods were allowed to precipitate. This precipitate was washed as mentioned above. Stable nanorods solutions were obtained after addition of a chloroform:*n*-propylamine mixture (10 mL, 2 vol. % *n*-propylamine).

ZnO:MDMO−PPV Blends. Blends of MDMO−PPV and ZnO were prepared starting by dissolving MDMO−PPV in chlorobenzene. The exact amount of the ZnO nanoparticle stock solution needed to reach the desired amounts of ZnO in the blends was determined from the ZnO concentration in the sol. This ZnO concentration was determined from the solid residue after solvent evaporation. The ZnO solution was used within three days after synthesis, because this led to the best cells with the highest reproducibility. On average a ZnO concentration of 65 mg mL^{-1} had been obtained. In a typical procedure, MDMO−PPV (3 mg) was dissolved in chlorobenzene (0.5 mL). For a 26 vol. % ZnO:MDMO−PPV blend (an MDMO−PPV: ZnO mass ratio of 1:2), 410 μL of a chlorobenzene:methanol mixture (v:v = 95:5) was added, followed by 90 μL of the ZnO

Bulk Heterojunction Solar Cells

J. Phys. Chem. B, Vol. 109, No. 19, 2005 **9515**

solution. The solution for spin coating contains approximately 4 vol. % methanol, calculated using a 20 vol. % methanol concentration for the ZnO solution. This procedure was followed because it led to a better dispersion of the ZnO in the polymer: chlorobenzene solution. Without the addition of methanol, prior to the addition of the ZnO solution, the nanoparticles could partially precipitate. The amount of methanol in the ZnO solution could be decreased down to 10% by centrifugation (when the amount of solvent added after centrifugation was kept constant to 10 mL). Lowering the amount of methanol led to unstable solutions because the ZnO nanoparticles precipitated.

Preparation of Photovoltaic Devices. Glass plates covered with patterned ITO resulting in 4 different device areas (0.095, 0.116, 0.37, and 1.02 cm^2) were used for device preparation. Photovoltaic devices were fabricated by spin casting a mixed solution in chlorobenzene (unless mentioned otherwise) of *nc*-ZnO and MDMO–PPV on a PEDOT:PSS film, which had been deposited on a UV ozone cleaned ITO coated glass substrate. *nc*-ZnO:MDMO–PPV composite films were spin cast between 500 and 3000 rpm for 2 min to vary the film thickness. All cast films were additionally dried at 2500 rpm for 1 min. Blends deposited from chloroform were spin cast for 1 min. The back electrode, consisting of 100 nm Al, was evaporated in high vacuum. Film thickness measurements were performed with a Tencor P10 surface profiler.

Current–Voltage Measurements. *J–V* measurements were performed in a N$_2$ atmosphere at room temperature. In forward bias, the ITO electrode was positively biased. The devices were illuminated at the transparent ITO electrode. *J–V* characteristics were measured with a computer-controlled Keithley 2400 Source Meter in the dark or under ∼85 mW cm^{-2} illumination from a 100-W tungsten–halogen lamp filtered by a Schott KG01 and GG420 filter providing a spectral range of 420–900 nm.

IPCE. Measurements were performed on a home-built setup, utilizing a xenon lamp and a Spex Minimate monochromator. The monochromatic light was focused on a diaphragm (2 mm diameter) to create a small light spot. Light power intensity at 500 nm was 1 mW cm^{-2} as determined with a calibrated Melles-Griot silicon diode. Currents were recorded using a Keithley 2400 Source Meter. Light intensity modulated data were recorded with a chopper at 80 Hz using a lock-in amplifier. Experiments with backlight were recorded by illumination of the solar cell with a continuous backlight of 30 mW cm^{-2} and intensity modulated monochromatic light.

UV–vis Absorption and Photoluminescence Spectroscopy. UV–vis spectra were recorded on a Perkin-Elmer Lambda 900 spectrophotometer. Photoluminescence spectra were recorded on an Edinburgh Instruments FS920 double-monochromator spectrometer with a Peltier-cooled red-sensitive photomultiplier. Time-correlated single photon counting photoluminescence studies were performed using an Edinburgh Instruments LifeSpec-PS consisting of a 400-nm picosecond (pulse width ∼50 ps) laser (PicoQuant PDL 800B) operated at 2.5 MHz and a Peltier-cooled Hamamatsu microchannel plate photomultiplier (R3809U-50). The *nc*-ZnO:MDMO–PPV blends from chlorobenzene solution (contained 3 mg mL^{-1} MDMO–PPV) were cast (at 1500 rpm) onto PEDOT:PSS covered ITO plates, for the UV–vis experiments, and on glass plates for the photoluminescence experiments.

Near-Steady-State Photoinduced Absorption. Spectra were recorded between 0.25 and 3 eV by exciting an *nc*-ZnO:MDMO–PPV film on quartz in an Oxford Optistat continuous flow cryostat at 80 K with a mechanically modulated (275 Hz) Ar-ion laser (Spectra Physics 2025) pump beam tuned to 488 nm (25 mW, beam diameter of 2 mm) and monitoring the resulting change in transmission (ΔT) of a tungsten–halogen white-light probe beam after dispersion by a triple-grating monochromator, using Si, InGaAs, and (cooled) InSb detectors. For PIA experiments, the UV lines (363 and 350 nm) of the Ar-ion laser were used.

Femtosecond Pump–Probe Spectroscopy. The femtosecond laser system used for pump–probe experiments consisted of an amplified Ti/sapphire laser (Spectra Physics Hurricane), providing 150-fs pulses at 800 nm with an energy of 750 μJ and a repetition rate of 1 kHz. The pump pulses (510 nm) were created via optical parametric amplification (OPA) of the 800 nm and frequency doubling. The probe beam (2200 nm) was generated in a separate OPA. The pump beam was linearly polarized at the magic angle (54.7°) with respect to the probe beam to cancel out orientation effects in the measured dynamics. The temporal evolution of the differential transmission was recorded using a cooled InSb detector by a standard lock-in technique at 500 Hz.

Nanosecond Transient Spectroscopy. Thin films of the *nc*-ZnO:MDMO–PPV composite material were obtained by spin coating from chlorobenzene solution on a quartz substrate. Transient spectra were recorded by exciting the sample with pulses at 450 nm (pulse width 4 ns, repetition rate 10 Hz) obtained from an optical parametric oscillator, pumped by the third harmonic of a Nd:YAG laser. The excited area was 1.8 mm^2, and the sample was held at 295 K in a flow cryostat in a N$_2$ atmosphere. An intensified charge-coupled device camera was used to record the transmission of a tungsten–halogen probe light through the sample after dispersion by a spectrograph. The signal acquisition by the camera was electronically gated. To obtain differential transmission spectra, the probe light was recorded at the delay time of interest and then the reference transmission at a 25 ms delay. For short acquisition delay times, the transmission spectra were corrected for a very small residual fluorescence.

TEM. A 1000× diluted solution of the nanoparticles or rods in dichloromethane was drop cast on a carbon-coated copper TEM grid. Films for TEM were prepared by flotation onto the surface of deionized water and picked up by a 400 mesh copper grid. The TEM observations were conducted on a JEOL JEM-2000FX transmission electron microscope operated at an acceleration voltage of 80 kV.

TM-AFM. TM-AFM measurements were performed on a Veeco MultiMode with a NanoScope IV controller, using TM-etched silicon cantilevers with a spring constant of 11.5 N/m and an apex radius of 10 nm.

References and Notes

(1) Schweitzer, B.; Bässler, H. *Synth. Met.* **2000**, *109*, 1.

(2) Yu, G.; Gao, J.; Hummelen, J. C.; Wudl, F.; Heeger, A. J. *Science* **1995**, *270*, 1789.

(3) Shaheen, S. E.; Brabec, C. J.; Padinger, F.; Fromherz, T.; Hummelen, J. C.; Sariciftci, N. S. *Appl. Phys. Lett.* **2001**, *78*, 841.

(4) Wienk, M. M.; Kroon, J. M.; Verhees, W. J. H.; Knol, J.; Hummelen, J. C.; Van Hal, P. A.; Janssen, R. A. J. *Angew. Chem., Int. Ed.* **2003**, *42*, 3371.

(5) Schilinsky, P.; Waldauf, C.; Brabec, C. J. *Appl. Phys. Lett.* **2002**, *81*, 3885.

(6) Svensson, M.; Zhang, F.; Veenstra, S. C.; Verhees, W. J. H.; Hummelen, J. C.; Kroon, J. M.; Inganäs, O.; Andersson, M. R. *Adv. Mater.* **2003**, *15*, 988.

(7) Brabec, C. J. *Sol. Energy Mater. Sol. Cells* **2004**, *83*, 273.

(8) Halls, Walsh, C. A.; Greenham, N. C.; Marseglia, E. A.; Friend, R. H.; Moratti, S. C.; Holmes, A. B. *Nature* **1995**, *376*, 498.

(9) Halls, J. J. M.; Arias, A. C.; MacKenzie, J. D.; Wu, W.; Inbasekaran, M.; Woo, E. P.; Friend, R. H. *Adv. Mater.* **2002**, *12*, 498.

(10) Veenstra, S. C.; Verhees, W. J. H.; Kroon, J. M.; Koetse, M. M.; Sweelssen, J.; Bastiaansen, J. J. A. M.; Schoo, H. F. M.; Yang, X.; Alexeev, A.; Loos, J.; Schubert, U. S.; Wienk, M. M. *Chem. Mater.* **2004**, *16*, 2503.

(11) Schmidt-Mende, L.; Frechtenkötter, A.; Müllen, K.; Moons, E.; Friend, R. H.; MacKenzie, J. D. *Science* **2001**, *293*, 1119.

(12) Ouali, L.; Krasnikov, V. V.; Stalmach, U.; Hadziioannou, G. *Adv. Mater.* **1999**, *11*, 1515.

(13) Melzer, C.; Krasnikov, V. V.; Hadziioannou, G. *Appl. Phys. Lett.* **2003**, *82*, 3101.

(14) Uchida, S.; Xue, J.; Rand, B. P.; Forrest, S. R. *Appl. Phys. Lett.* **2004**, *84*, 4218.

(15) Peumans, P.; Uchida, S.; Forrest, S. R. *Nature* **2003**, *425*, 158.

(16) Xue, J.; Uchida, S.; Rand, B. P.; Forrest, S. R. *Appl. Phys. Lett.* **2004**, *85*, 5757.

(17) Greenham, N. C.; Peng, X.; Alivisatos, A. P. *Phys. Rev. B* **1996**, *54*, 17628.

(18) Huynh, W. U.; Peng, X.; Alivisatos, A. P. *Adv. Mater.* **1999**, *11*, 923.

(19) Huynh, W. U.; Dittmer, J. J.; Alivisatos, A. P. *Science* **2002**, *295*, 2425.

(20) Sun, B.; Marx, E.; Greenham, N. C. *Nano Lett.* **2003**, *3*, 961.

(21) Sun, B.; Snaith, H. J.; Dhoot, A. S.; Westenhoff, S.; Greenham, N. C. *J. Appl. Phys.* **2005**, *97*, 014941.

(22) Kwong, C. Y.; Djurisic, A. B.; Chui, P. C.; Cheng, K. W.; Chan, W. K. *Chem. Phys. Lett.* **2004**, *384*, 372.

(23) Beek, W. J. E.; Wienk, M. M.; Janssen, R. A. J. *Adv. Mater.* **2004**, *16*, 1009.

(24) FF is defined as the ratio of the product of current density and voltage in the MPP and the product of short circuit current (J_{SC}) and open circuit voltage (V_{OC}): FF = $(J_{MPP} \times V_{MPP})/(J_{SC} \times V_{OC})$.

(25) Arias, A. C.; MacKenzie, J. D.; Stevenson, R.; Halls, J. J. M.; Inbasekaran, M.; Woo, E. P.; Richards, D.; Friend, R. H. *Macromolecules* **2001**, *34*, 6005.

(26) Snaith, H. J.; Arias, A. C.; Morteani, A. C.; Silva, C.; Friend, R. H. *Nano Lett.* **2002**, *2*, 1353.

(27) Huynh, W. U.; Dittmer, J. J.; Libby, W. C.; Whiting, G. L.; Alivisatos, A. P. *Adv. Funct. Mater.* **2003**, *13*, 73.

(28) Van Duren, J. K. J.; Yang, X.; Loos, J.; Bulle-Lieuwma, C. W. T.; Sieval, A. B.; Hummelen, J. C.; Janssen, R. A. J. *Adv. Funct. Mater.* **2004**, *14*, 425.

(29) Hoppe, H.; Niggemann, M.; Winder, C.; Kraut, J.; Hiesgen, R.; Hinsch, A.; Meissner, D. Sariciftci, N. S. *Adv. Funct. Mater.* **2004**, *14*, 1005.

(30) Pacholski, C.; Kornowski, A.; Weller, H. *Angew. Chem., Int. Ed.* **2002**, *41*, 1188.

(31) Haase, M.; Weller, H.; Henglein, A. *J. Phys. Chem.* **1988**, *92*, 482.

(32) Meulenkamp, E. A. *J. Phys. Chem. B.* **1998**, *102*, 5566.

(33) $\lambda_{1/2}$ is defined as the wavelength at which the absorption was 50% of that at the shoulder (exitonic peak) shown in Figure 1b.

(34) Use of: $1240/\lambda_{1/2} = 3.301 + 294/D^2 + 1.09/D$, $\lambda_{1/2} = 360$ nm (see Figure 3.3a).

(35) The correct positions (in 2θ) for the peaks are: 31.8 (100), 34.5 (002), 36.3 (101), 47.5 (102), 56.6 (110), and 62.9° (103). Calculated using the ICSD database http://www.cmbi.kun.nl/icsd: Albertsson, J.; Abrahams, S. C.; Kvick, A. *Acta Crystallogr. B.* **1983**, *45*, 34.

(36) Wei, X.; Vardeny, Z. V.; Sariciftci, N. S.; Heeger, A. J. *Phys. Rev. B.* **1996**, *53*, 2187.

(37) Shim, M.; Guyot-Sionnest, P. *J. Am. Chem. Soc.* **2001**, *123*, 11651.

(38) Pientka, M.; Dyakonov, V.; Meissner, D.; Rogach, A.; Talapin, D.; Weller, H.; Lutsen, L.; Vanderzande, D. *Nanotechnology* **2004**, *15*, 163.

(39) The ZnO nanoparticle film was deposited at the inside of a quartz NIR cell and sealed in a glovebox, to exclude the oxygen.

(40) Katoh, R.; Furube, A.; Hara, K.; Murata, S.; Sugihara, H.; Arakawa, H.; Tachiya, M. *J. Phys. Chem. B* **2002**, *106*, 12957.

(41) Van Dijken, A.; Meulenkamp, E. A.; Vanmaekelbergh, D.; Meijerink, A. *J. Lumin.* **2000**, *90*, 123.

(42) Van Dijken, A.; Meulenkamp, E. A.; Vanmaekelbergh, D.; Meijerink, A *J. Lumin.* **2000**, *87−89*, 454.

(43) Bauer, C.; Boschloo, G.; Mukhtar, E.; Hagfeldt A. *J. Phys. Chem. B* **2001**, *105*, 5585.

(44) Offermans, T.; Meskers, S. C. J.; Janssen, R. A. J. *J. Chem. Phys.* **2003**, *119*, 10924.

(45) The vol. % of ZnO was determined from the amount of ZnO and MDMO−PPV in the solution using the densities of ZnO (5.6 mg mL^{-1}) and MDMO−PPV (0.91 mg mL^{-1}).

(46) Savenije, T. J.; Kroeze, J. E.; Wienk, M. M.; Kroon, J. M.; Warman, J. M. *Phys. Rev. B* **2004**, *69*, 155205.

(47) Srikant, V.; Clarke, D. R. *J. Appl. Phys.* **1998**, *83*, 5447.

(48) Vossmeyer, T.; Katsikas, L.; Giersig, M.; Popovic, I. G.; Diesner, K.; Chemseddine, A.; Eychmüller, A.; Weller, H. *J. Phys. Chem.* **1994**, *98*, 7665.

(49) The relative humidity of the surrounding atmosphere during spin coating seemed to influence the film thickness and the solar cell performance. These effects have not been investigated in great detail, but films cast at high humidity appeared 40 nm thinner than those cast at low humidity.

(50) The intensity was determined by comparing the measured J_{SC} with the J_{SC} at 1 sun intensity, which was obtained from the convolution of the spectral response with the solar AM1.5 spectrum and correcting for the small nonlinearity of the light intensity dependence using $I = I(1 \text{ sun}) \times [J_{SC}/J_{SC}(1 \text{ sun})]^{1/n}$ with $n = 0.93$.

(51) Wang, Y.; Song, R.; Li, Y.; Shen, J. *Surf. Sci.* **2003**, *530*, 136.

(52) Knoll, A.; Magerle, R.; Krausch, G. *Macromolecules* **2001**, *34*, 4159.

(53) Basnar, B.; Friedbacher, G.; Brunner, H.; Vallant, T.; Mayer, U.; Hoffmann, H. *Appl. Surf. Sci.* **2001**, *171*, 213.

(54) Feng, J.; Weng, L.-T.; Chan, C.-M.; Xhie, J.; Li, L. *Polymer* **2001**, *42*, 2259.

(55) Cleveland, J. P.; Ancykowski, B.; Schmid, A. E.; Elings, V. B. *Appl. Phys. Lett.* **1998**, *72*, 2613.

(56) Garcia, R.; Tamajo, J.; Calleja, M.; Garcia. F. *Appl. Phys. A* **1998**, *66*, S309.

(57) Pacholski, C. Thesis, Hamburg University, July 2002.